Available online at www.sciencedirect.com

SciVerse ScienceDirect

Ceramics International 39 (2013) 3313–3320

CERAMICS INTERNATIONAL

www.elsevier.com/locate/ceramint

Microstructural, corrosion and nanomechanical behaviour of ceramic coatings developed on magnesium AZ31 alloy by micro arc oxidation

Arjun Dey[a], R.Uma Rani[a,*], Hari Krishna Thota[a], Anand Kumar Sharma[a], Payel Bandyopadhyay[b], Anoop Kumar Mukhopadhyay[b]

[a]*Thermal Systems Group, ISRO Satellite Centre, Vimanapura Post, Bangalore-560 017, India*
[b]*Mechanical Property Evaluation Section, CSIR-Central Glass and Ceramic Research Institute, Kolkata-700 032, India*

Received 27 June 2012; received in revised form 4 October 2012; accepted 5 October 2012
Available online 17 October 2012

Abstract

Microstructural, corrosion and nanomechanical behaviour of micro arc oxidised (MAO) coating grown on magnesium AZ31B alloy was evaluated. Microstructural characterization of the coating was carried out by X-ray diffraction (XRD), scanning electron microscopy (SEM) followed by image analysis and energy dispersive spectroscopy (EDX). Linear polarization technique was used to evaluate the corrosion behaviour of the MAO coating. Further, nanoindentation was employed to evaluate nanohardness and Young's modulus of the MAO coating. The characteristic values of both the nanohardness and the Young's modulus were calculated through the application of the Weibull statistics.

Keywords: Micro arc oxidation; Microstructure; Nanoindentation; Linear polarization

1. Introduction

Magnesium (Mg) alloys have many merits like light weight, high strength, good ductility etc. and hence are considered as one of the most prospective candidate for space applications. However, often the actual application is limited due to the poor corrosion resistance and surface mechanical properties of these alloys. Therefore, a lot of studies have been going on to improve the aforesaid properties by different surface treatments or modifications like chemical conversion [1], anodizing [2], micro arc oxidation (MAO) [3], ion implantation [4], laser treatments [5] and so on. However, every method has its own merits and demerits. Commercially, MAO is being widely used for surface modification of Mg alloy due to better reliability and economical advantages for the spacecraft application [6]. Further, environmentally friendly electrolytes are used to produce MAO coating on magnesium and its alloys which are generally based on mainly alkaline solutions of aluminates, phosphates, silicates etc. [7–19]. Most of these researches focused on the influence of a single electrolyte or a mixed electrolyte systems on the structural as well corrosion properties of anodic films formed on Mg. However, the in depth understanding of mechanical properties at the local microstructural length scale is not yet explored. Moreover, generally MAO coatings consist of porous and micro-cracked morphology which produce a heterogeneous microstructure [20–22]. Therefore, it is challenging as well as important to measure the mechanical properties such as hardness and Young's modulus at the local microstructural length scale because any mechanical disintegration starts from the sub-micron scale of the microstructure. It was also found in general that the scatter in the nanoindentation data was very high for the MAO coatings, presumably due to the highly heterogeneous and porous structure of the coatings [20–23]. Very few literatures are available for MAO coatings on aluminum and Ti alloys [21–23] where the researchers focussed the issue of data scatter. However, there is no reported literature available which addressed and studied this problem related to MAO coatings on Mg alloys.

*Corresponding author. Tel.: +91 8025037404.
E-mail address: rurani@isac.gov.in (R.Uma Rani).

0272-8842/$ - see front matter © 2012 Elsevier Ltd and Techna Group S.r.l. All rights reserved.
http://dx.doi.org/10.1016/j.ceramint.2012.10.020

The major objective of the present study was to characterize the nanohardness and elastic modulus of MAO coatings by the nanoindentation technique. Weibull statistical analysis has been utilized to obtain the characteristic values of nanohardness and Young's modulus for useful exploitation of structural designing.

2. Materials and methods

2.1. MAO coating preparation

In the present work, AZ31B Mg alloy ($50 \times 50 \times 12$ mm^3) with chemical composition of ~3 wt% Al, 1 wt% Zn and 96 wt% Mg was used as a substrate. Prior to the MAO process, the flat ground substrates were cleaned by ultrasonic cleaning using AR-grade acetone and dried in air. Further, a threaded hole with a diameter of 2.5 mm was applied on one of the top side of the specimens to obtain a stable current transfer through the sample and electrolyte.

Micro arc oxidation (MAO) coatings were obtained as per the reported procedure in an electrolyte system consisting of sodium silicate 30 g/L and sodium fluoride 10 g/L [7]. An AC power supply of 50 Hz frequency at a current density of 2.5 A/dm^2 for 15 min was used for both electrolyte systems. The temperature of the electrolyte was maintained at 27 ± 1 °C by a cooling system throughout the coating process.

In the MAO process, the coating is formed by the application of an electric field greater than the dielectric breakdown voltage of the initially formed oxide film. Due to this some dispersed discharges can be observed on the metal surface. The plasma chemical reactions occurring in the region of each discharge leads to conversion of the surface to a stable and protective oxide layer. More significantly, local conditions of heat and pressure, sinter, anneal and rapid cooling also modifies the state of the coating resulting in a complex mixture of amorphous and crystalline phases [24]. Further, to reduce the porosity of MAO coating, pore sealing was carried out by immersion of the as coated specimen in boiling water for 30 min. The as prepared silicate based MAO (S-MAO) samples are designated as SU-MAO while the sealed silicate based MAO samples are designated as SS-MAO.

2.2. Coating characterizations

2.2.1. Phase analysis

The phases of the coatings were determined by using X-ray diffraction (XRD) method. The experiments were performed using a commercial X-ray diffractometer (Philips X'pert-Pro instrument, monochromatic Cu $K_{\alpha 1}$ radiation, $\lambda = 1.5406$ A, 30 mA, 40 kV, The Netherlands). The scanning range of diffraction angle (2θ) was set between 30° and 80° with steps of 0.02° and a step time of 40 s.

2.2.2. Microstructural study

The microstructural characterizations were carried out by the scanning electron microscope (SEM: Leica S 440i, UK) operated at a voltage of 20 kV and a probe current of 100 pA. The filament current was 2.70 A and the detector used was a secondary electron detector. Elemental composition of the coatings was analyzed using energy dispersive X-ray spectroscopy (EDX: Oxford Instruments, INCA X-Max, U.K.) attached to the scanning electron microscope mentioned above. Further, the elemental mapping was studied by EDX. To avoid charging a 50–80 nm gold coating was deposited on the MAO samples by the arc deposition technique prior to insertion in the sample chamber for scanning electron microscopy.

2.2.3. Coating thickness and porosity measurement

The thickness of the MAO coating was measured by using an eddy-current coating thickness measurement gauge (Isoscope, Model MP 2B-T3 3B, Helmut Fischer, Germany). The resolution of the gauge is about 0.1 μm with a measurement ability of the coatings in the range of 1–200 μm. The average percentage of open porosity and the pore sizes were measured utilizing the image analysis technique in an image analyzer (Leica Q500MC, UK) for at least 5 SEM photomicrographs taken randomly from five different locations of the coating.

2.2.4. Corrosion behavior

The DC polarization tests were carried out using an Autolab PGSTAT 302 N potentiostat (Eco-chemie, The Netherlands). The cell used was a conventional three electrode set-up with the coated sample utilized as the working electrode. A platinum rod electrode was used as counter electrode and an Ag/AgCl, 3 M KCl electrode as the reference electrode. The tests were performed in air at room temperature in a ~3.5 wt% NaCl electrolytic solution. The edges of the samples were sealed with an acrylic resin. The exposed area within the testing solution was about 1 cm^2 and the samples were immersed in the corrosive media for 15 min before the polarization test. The anodic and cathodic polarization curves were recorded using a sweep potential test in the range ±100 mV with respect to the open circuit potential (OCP) with a scanning rate of 0.001 V/s.

The Tafel plots were obtained after electrochemical measurements. The corrosion potential (E_{corr}), the corrosion current density (i_{corr}) and polarization resistance (R_p) were deduced from the Tafel plot (i.e., log i vs E plot). The corrosion current is obtained using Stern–Geary equation [25]:

$$I_{corr} = b_a b_c / (b_a + b_c)\, 2.303 R_p \quad (1)$$

where I_{corr} is a corrosion current in μA/cm^2. Further, b_a and b_c are anodic and cathodic Tafel slopes, respectively expressed in V/decade, R_p is a polarization resistance expressed in Ω cm^2. The polarization resistance is calculated using the following

relation:

$$R_p = \frac{\Delta E}{\Delta i}\Big|_{\Delta E \to 0} \quad (2)$$

where ΔE is the polarization potential and Δi is the polarization current. If the corrosion current decreases the polarization resistance increases.

2.2.5. Nanoindentation study

Prior to the nanoindentation study, the surfaces of the MAO coating were polished with the diamond pastes (Eastern Diamond Products Pvt. Ltd, Kolkata, India) of 3, 1, and 0.25 μm grit sizes and finally with a silica suspension ($d_{50} - 0.04$ μm). A commercial nanoindentation machine (Fischerscope H100-XYp; Fischer, Switzerland) equipped with a Berkovich indenter was employed for measuring nanohardness (H) and Young's modulus. The machine worked according to DIN 50359-1 standard. The depth and force sensing resolutions of the machine were 1 nm and 0.2 μN, respectively. The machine was calibrated with nanoindentation based independent evaluation of nanohardness, H -4.14 ± 0.1 GPa and Young's modulus, E -84.6 ± 3.5 GPa of a standard reference block, e.g., Schott BK7 Glass (Schott, Germany) provided by the supplier. The experiments were conducted at a constant load of 100 mN. The Berkovich indenter had a tip radius of about 150 nm and a semi-apex angle of 65.3°. Both the loading and unloading times were kept fixed at 30 s. The measurements of H and E were done from the experimentally obtained load versus depth of penetration plots using the well known Oliver and Pharr method [26]. At least twenty indents were made at five different locations of the sample as the nature of the surface of the coating was porous and heterogeneous. The measurements were taken well below the 10% of the coating thickness such that there would not be any influence of the substrate's mechanical properties on the measured data.

The high characteristic scatter in data for both E and H of the highly porous and heterogeneous MAO coating was treated with the well-established Weibull distribution. This statistical method has been widely employed to determine the characteristics values for the micro-/nano hardness and Young's modulus of heterogeneous brittle coatings like thermal barrier coatings [27–29] and microplasma sprayed hydroxyapatite coatings [30,31]. The two-parameter Weibull model provides the survival probability, p, for a given parameter, x [27–31]. In the present study, x will be nanohardness (H) and Young's modulus (E). It also provides in addition the Weibull modulus (m), a dimensionless quantity that reflects the degree of scatter in the data within the distribution. It's magnitude increases with decrease in scatter of the data [27–31]. In addition, the Weibull analysis provides the characteristic value (x_{ch}) of the related parameter, x [30,31]. The characteristic values are of immense engineering significance as it provides the designer with a unique and dependable value of the required parameter that has a 63.2% probability of occurrence.

3. Results and discussions

The thickness of the coating as measured by eddy-current method was 30.1 ± 2.2 μm. The data on the phase compositions of SU-MAO and SS-MAO coatings are presented in Fig. 1(a and b), respectively. X-ray diffraction (XRD) analyses indicated that the MAO coating produced in silicate electrolyte (S-MAO) was composed predominantly of Mg_2SiO_4 (ICSD code: 00-034-0189), Mg_2SiO_3 (ICSD code: 00-034-1216) and MgO (ICSD code: 00-045-0946, 00-004-0829) [7,10–12,15]. According to the relative intensity of the peaks in XRD, it was observed that Mg_2SiO_4 was the main phase in the *S*-MAO coating. Further, MgO phase was formed when Mg^{2+} cations react with O^{2-} anions under the high temperature and pressure due to the existence of electric field during MAO [11,12] where as Mg_2SiO_4 phase forms in the coating structure when MgO and SiO_2 react under the high temperature [10,19]. Moreover, the Mg peaks were also observed because through the porosity in the coating the substrate was exposed in a localized manner to the incident X-ray beam. This was also reported by the others [10].

SEM photomicrographs of the SU-MAO and SS-MAO are shown in Fig. 2(a and b), respectively. The coatings show the characteristic presence of the pores as well as microcracks [20–22]. The formation of the MAO coating is based on the sparks passing through the oxide layer and generating the discharge tunnels [10,12,20]. Thus, the nature of the coating formation introduces pores in the surface of the coating.

Based on the image analysis data as mentioned above, the percentage values of open porosity and equivalent diameter of the pore of SU-MAO and SS-MAO samples are shown in Table 1. The data revealed that after sealing, the open porosity as well as the equivalent diameter of the pores was reduced marginally.

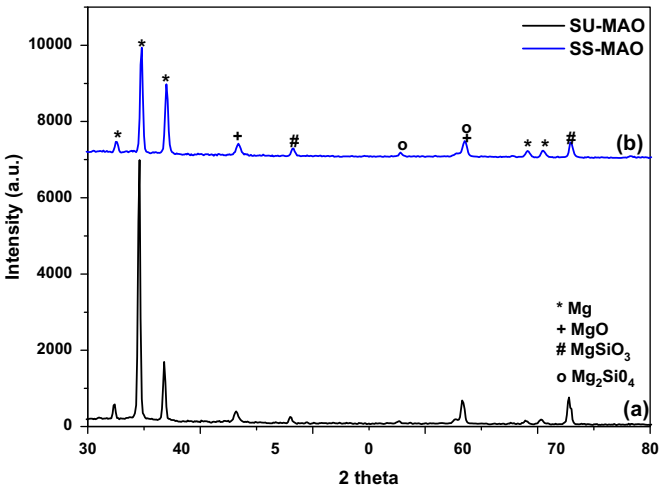

Fig. 1. XRD pattern of (a) SU-MAO and (b) SS-MAO.

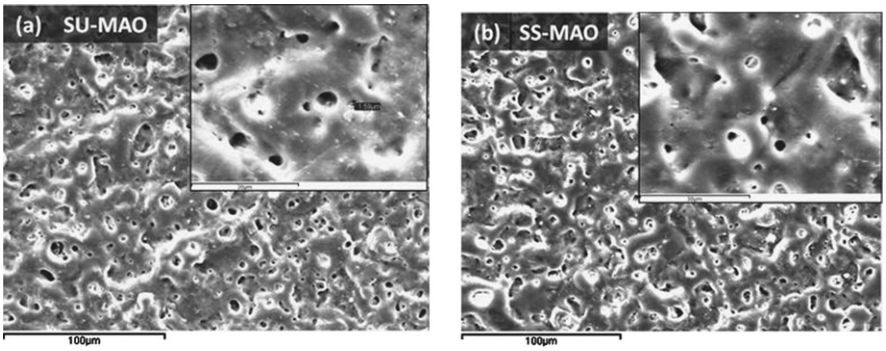

Fig. 2. SEM photomicrographs of the (a) SU-MAO and (b) SS-MAO (inset-higher magnification images).

Table 1
Porosity and Equivalent pore diameter of the SU-MAO and SS-MAO coatings.

Sample name	Open porosity (Vol%)	Equivalent diameter of the pore (μm)
SU-MAO	4.28 ± 0.53	2.97 ± 1.33
SS-MAO	4.03 ± 0.43	2.76 ± 1.41

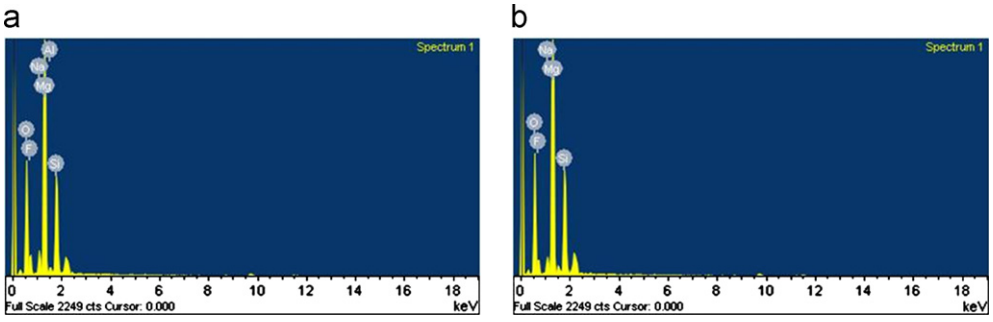

Fig. 3. EDX spectra of (a) SU-MAO and (b) SS-MAO.

Table 2
Chemical composition analysis on plan section of the MAO coatings.

Sample Name	Elements											
	F		Na		Mg		Al		Si		O	
	Wt. (%)	At. (%)	Wt. (%)	At. (%)	Wt. (%)	At. (%)	Wt. (%)	At. (%)	Wt. (%)	At. (%)	Wt. (%)	At. (%)
SU-MAO	14.39	15.12	3.32	2.80	30.13	24.75	0.84	0.62	13.89	9.88	37.52	46.83
SS-MAO	10.87	11.44	2.16	1.88	32.61	26.82	0.78	0.54	15.02	10.70	39.33	49.16

EDX spectrum of the SU-MAO and SS-MAO are shown in Fig. 3(a and b), respectively. MAO coatings showed (Fig. 3) the dominant magnesium and oxygen peaks as expected. Further, sodium and fluorine peaks were also observed from the starting precursor bath [10]. As expected, silicon peak was pronounced for the silicate bath based MAO coatings [11]. Moreover, the aluminum peak might possibly have had arisen from the base Mg alloy [11]. Further, both the atomic and the weight percentages of each element are shown in Table 2.

The protectiveness of the MAO coating and the composite coatings were evaluated through the potentiodynamic polarization tests in a 3.5 wt% NaCl solution as mentioned above. The polarization curves for SU-MAO and SS-MAO coatings are shown in Fig. 4(a and b), respectively. The electrochemical parameters of the potentiodynamic polarization

are summarized in Table 3. Among these parameters, corrosion potential (E_{corr}), polarization resistance (R_p) and anodic/cathodic Tafel slopes (b_a and b_c) were derived directly from the experimentally measured polarization curves. The corrosion current density (I_{corr}) was calculated by Stern–Geary equation [32].

These data clearly showed that the corrosion resistance of SS-MAO is enhanced to a great extent. The SU-MAO coating exhibits a corrosion potential of ~ -1.62 V, higher corrosion current ($\sim 5.9 \times 10^{-7}$ A/cm^2) and lesser R_p value whereas the SS-MAO coating exhibits a corrosion potential of -1.50 V, lower corrosion current ($\sim 2.9 \times 10^{-7}$ A/cm^2) and higher R_p value. The increase in the corrosion potential, decrease in corrosion current of SS-MAO and increase in R_p value can be qualitatively explained by the closure of pores of the unsealed SU-MAO coating during hydrothermal sealing.

The typical load–depth (P–h) plots of the MAO coatings are shown in Fig. 5. Generally, the p–h plots showed the normal behavior both in case of SU-MAO and SS-MAO. The general nature of these plots indicated the presence of an elastic-plastic deformation process as expected for brittle materials. Further, the irregular behavior of P–h plot was also observed due to influence of defects like pore and microcracks in the MAO coatings which is the characteristic of MAO process. Moreover, there was also a pronounced presence of 'pop-in' due to interaction of pores.

As mentioned above, the coatings possess porosity and heterogeneity. Due to this microstructural peculiarity, the mechanical characterization of such a coating is obviously rendered very difficult. That is why it was decided to employ a Weibull statistical approach so that characteristic values of both nanohardness and Young's modulus can be obtained prior to and post immersion of coating into the corrosive environment.

Weibull distribution fittings for the nanohardness and Young's modulus data of the MAO coatings are displayed in Fig. 6(a and b), respectively for as grown condition (i.e., before the immersion into the corrosion environment.). Similarly, Weibull distribution fittings for the nanohardness and Young's modulus data of the MAO coatings are displayed in Fig. 7(a and b), respectively after the immersion into the corrosion environment.

The characteristic values of nanohardness and Young's modulus were calculated from this data through the application of Weibull statistics, following references [27–31]. As mentioned earlier, values of both nanohardness and Young's modulus can be obtained in the cases of both prior and post immersion into the corrosive environment. The characteristic nanohardness (H_{char}) value was ~ 3 GPa. After the immersion into the corrosive environment the magnitude of H_{char} was marginally reduced for both sealed as well as unsealed MAO coatings (Table 4). Further, sealing of MAO samples showed no improvement of nanohardness, however, it showed marginal improvement of the Young's modulus. On the other hand, the characteristic Young's modulus, E_{char} (~ 90 GPa) of unsealed MAO coatings was not altered after immersing into the corrosion environment. In contrast, the sealed MAO coatings showed E_{char} of ~ 96 GPa which was marginally decreased to ~ 94 GPa when exposed to the corrosive environment (Table 5). Here, the reported hardness and Young's modulus of Mg alloy are in the range of 0.5 to 0.75 GPa and of 45 to 50 GPa, respectively [13,32]. Thus, the surface mechanical properties e.g., nanohardness and Young's

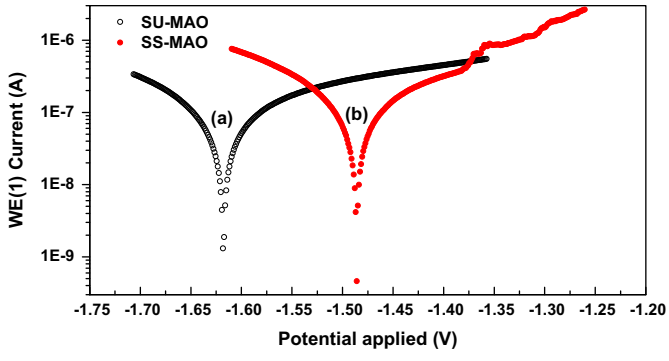

Fig. 4. Potentiodynamic polarization curves for (a) SU-MAO and (b) SS-MAO.

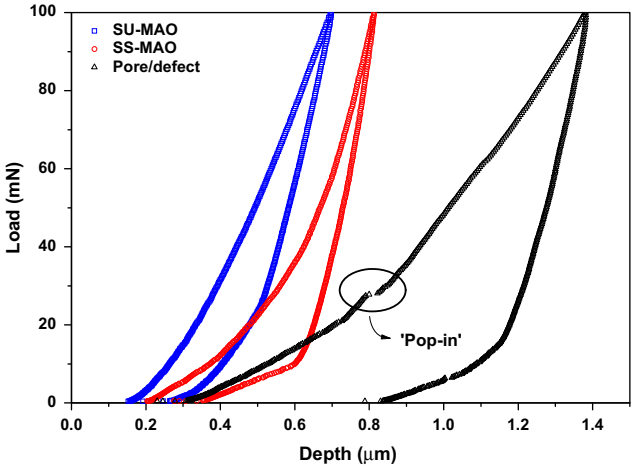

Fig. 5. Typical load-depth (P–h) plots of the various MAO coatings.

Table 3
Linear polarization data of the MAO coatings on Mg AZ31B alloy.

Sample name	b_a (V/dec)	b_c (V/dec)	E_{corr} (V)	I_{corr} (A/cm^2)	R_p (Ω/cm^2)
SU-MAO	0.052972	0.042362	−1.6176	5.8996×10^{-7}	229,560
SS- MAO	0.061186	0.040771	−1.4859	2.9019×10^{-7}	329,210

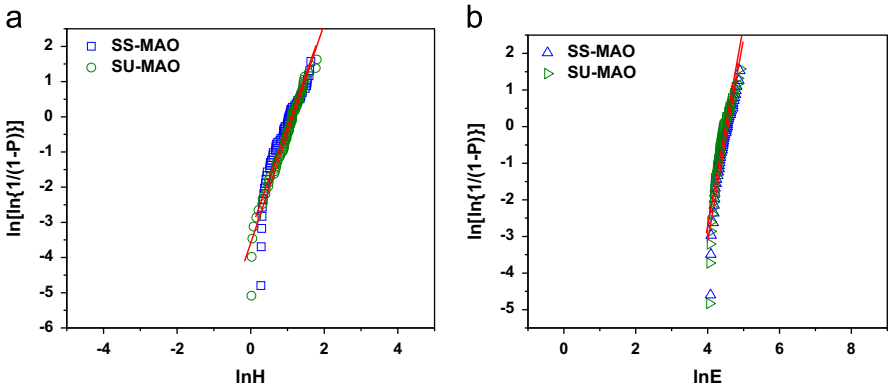

Fig. 6. Weibull plots of (a) nanohardness and (b) Young's modulus data of MAO coatings prior to the corrosion test.

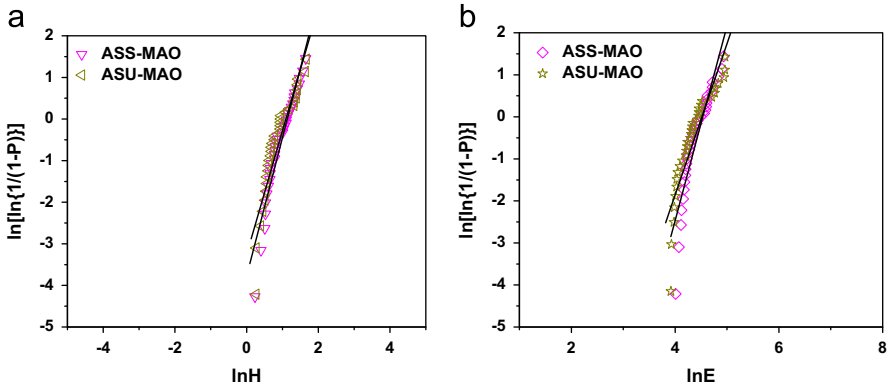

Fig. 7. Weibull plots of (a) nanohardness and (b) Young's modulus data of MAO coatings after the corrosion test.

Table 4
Weibull analysis data for the nanohardness of the MAO coatings.

Sample name	H_{char} (GPa)	m	Correlation coefficient (R^2)
SU-MAO	3.09	3.1	0.97
SS-MAO	3.11	2.9	0.88
ASU-MAO*	3.04	2.9	0.86
ASS-MAO**	3.09	3.3	0.92

*ASU-MAO=SU-MAO coating after the corrosion test.
**ASS-MAO=SS-MAO coating after the corrosion test.

Table 5
Weibull analyis data for the Young's modulus of the MAO coatings.

Sample name	E_{char} (GPa)	m	Correlation coefficient (R^2)
SU-MAO	90.23	5.5	0.85
SS-MAO	96.42	5.6	0.91
ASU-MAO*	90.02	3.6	0.83
ASS-MAO**	93.87	4.6	0.85

*ASU-MAO=SU-MAO coating after the corrosion test.
**ASS-MAO=SS-MAO coating after the corrosion test.

modulus of Mg alloy were improved after the MAO process. Further, silicate based MAO coating on Mg alloy showed the hardness of 5.12 GPa [33] and 6.5 GPa [34] measured by Vickers indentation. Narulkar et al. [35] reported ~4.01 GPa hardness measured by Vickers indentation on MAO coatings on Mg alloy prepared by Na_2SiO_3–Na_2WO_4–KOH–Na_2EDTA electrolyte. This MAO coating comprised of MgO, $MgAl_2O_4$ and $MgSiO_3$ phases. However, nanoindentation technique applied to the MAO coating on Mg alloys prepared by $KMnO_4$ electrolyte showed nanohardness in the range of 1.5 to 6.7 GPa [36]. This MAO coating possessed MgO and Mn_2O_3 phases [36]. Therefore, it appears that our measured nanohardness value was slightly lower than those reported in the earlier literatures [13,33–36]. However, these researchers [13,33–36] neither took the porous and heterogeneous microstructure of MAO coatings into account nor introduced the Weibull approach. Moreover, the type of Mg alloy substrate, electrolyte as well as MAO process parameters are also different from the present report.

Further, the 'm' value of nanohardness for the present MAO coatings were ~3 (Table 4) irrespective of whether it was sealed or not and whether the condition is prior to or post immersion into the corrosive environment. However, 'm' value of Young's modulus was in the range of ~3.5 to 5.5 (Table 5). These low values signify a high degree of scatter in the data. This was nothing unexpected because the coatings characteristically had a statistical distribution of defects e.g., pores and cracks/microcracks [20–22]. In post immersion condition into the corrosive environment, the 'm' values for both the nanohardness as well as Young's modulus decreased with respect to those obtained prior to the immersion.

This observation means that the defect density increases in post immersion condition over and above that which was already exist in the microstructure. Due to higher defect density in the post immersion condition more scatter is introduced into the data. This process lead to the further reduction of the "*m*" values in comparison to those obtained prior to immersion in the corrosive environment.

4. Conclusions

Surface modifications of magnesium AZ31B alloy were performed by the MAO process with silicate electrolyte. The MAO coating comprised of the MgO, Mg_2SiO_4 and Mg_2SiO_3 phases as indicated by the XRD data. The coating had $4.28 \pm 0.53\%$ open porosity and 2.97 ± 1.33 μm equivalent diameters of the pores as revealed by image analysis data. Both these parameters were reduced after the sealing process to $4.03 \pm 0.43\%$ and 2.76 ± 1.41 μm, respectively. The characteristic values of nanohardness and Young's modulus of the MAO coatings were evaluated through the Weibull approach to be ~3 and ~90 GPa, respectively. Further, sealing of MAO samples showed only a marginal improvement of Young's modulus while the nanohardness remained as good as that of the unsealed coating. However, the sealed coating performed much better than the unsealed one in the corrosive environment. Most importantly there was no significant degradation of nanohardness and Young's modulus of the coatings after the immersion into the corrosive environment. The characteristic heterogeneous microstructure of the coatings had many pores and cracks which lead to high scatter of data due to the interaction of the nanoindentation cavity volume and the spatial statistical distribution of the characteristic defects present in the coating and consequently to low values (e.g., ~3–6) of the Weibull modulus for both nanohardness and Young's modulus, as expected.

References

[1] H. Meifeng, L. Lei, W. Yating, T. Zhixin, H. Wenbin, Corrosion properties of surface-modified AZ91D magnesium alloy, Corrosion Science 50 (2008) 3267–3273.

[2] T. Lei, C. Ouyang, W. Tang, L.-F. Li, L.-S. Zhou, Preparation of MgO coatings on magnesium alloys for corrosion protection, Surface and Coatings Technology 204 (2010) 3798–3803.

[3] P. Liu, X. Pan, W. Yang, K. Cai, Y. Chen, Improved anticorrosion of magnesium alloy via layer-by-layer self-assembly technique combined with micro-arc oxidation, Materials Letters 75 (2012) 118–121.

[4] I. Nakatsugawa, R. Martin, E.J. Knystautas, Improving corrosion resistance of AZ91D magnesium alloy by nitrogen ion implantation, Corrosion 52 (1996) 921–926.

[5] L.A. Dobrzański, J. Domaga, T. Tański, A. Klimpel, D. Janicki, Laser surface treatment of magnesium alloy with WC powder, Archives of Materials Science and Engineering 30 (2008) 113–116.

[6] S. Shrestha, B.D. Dunn, Surface modification of light alloys by plasma electrolytic oxidation and anodising processes—spacecraft applications, in: H. Dong (Ed.), Surface Engineering of Light Alloys Al, Mg and Ti Alloys, Woodhead Publishing Ltd., 2010, pp. 603–641.

[7] H. Zhao, Z. Liu, Z. Han, A Comparison on ceramic coating formed on AM50 Alloy by micro-arc oxidation in two electrolytes, Materials Science Forum 546–549 (2007) 575–578.

[8] Y.K. Pan, C.Z. Chen, D.G. Wang, X. Yu, Z.Q. Lin, Influence of additives on microstructure and property of microarc oxidized Mg–Si–O coatings, Ceramics International (2012) in press.

[9] H.M. Wang, Z.H. Chen, L.L. Li, Corrosion resistance and microstructure characteristics of plasma electrolytic oxidation coatings formed on AZ31 magnesium alloy, Surface Engineering 26 (2010) 385–391.

[10] P.B. Srinivasan, C. Blawert, M. Stormer, W. Dietzel, Characterisation of tribological and corrosion behaviour of plasma electrolytic oxidation coated AM50 magnesium alloy, Surface Engineering 26 (2010) 340–346.

[11] H.F. Guo, M.Z. An, H.B. Huo, S. Xu, L.J. Wu, Microstructure characteristic of ceramic coatings fabricated on magnesium alloys by micro-arc oxidation in alkaline silicate solutions, Applied Surface Science 252 (2006) 7911–7916.

[12] S. Durdu, A. Aytac, M. Usta, Characterization and corrosion behavior of ceramic coating on magnesium by micro-arc oxidation, Journal of Alloys and Compounds 509 (2011) 8601–8606.

[13] F. Jin, P.K. Chu, G. Xu, J. Zhao, D. Tang, H. Tong, Structure and mechanical properties of magnesium alloy treated by micro-arc discharge oxidation using direct current and high-frequency bipolar pulsing modes, Materials Science and Engineering A 435–436 (2006) 123–126.

[14] A. Da Forno, M. Bestetti, Effect of the electrolytic solution composition on the performance of micro-arc anodic oxidation films formed on AM60B magnesium alloy, Surface and Coatings Technology 205 (2010) 1783–1788.

[15] A. Ghasemi, N. Scharnagl, C. Blawert, W. Dietzel, K.U. Kainer, Influence of electrolyte constituents on corrosion behaviour of PEO coatings on magnesium alloys, Surface Engineering 26 (2010) 321–327.

[16] D. Chen, W. Li, J. Jie, Investigation of the anti-corrosion ceramic coating formed on AZ91D magnesium alloy by micro-arc oxidation, Key Engineering Materials 353–358 (2007) 1645–1648.

[17] D. Sreekanth, N. Rameshbabu, K. Venkateswarlu, Effect of various additives on morphology and corrosion behavior of ceramic coatings developed on AZ31 magnesium alloy by plasma electrolytic oxidation, Ceramics International 38 (2012) 4607–4615.

[18] P.B. Srinivasan, J. Liang, C. Blawert, M. Stormer, W. Dietzel, Development of decorative and corrosion resistant plasma electrolytic oxidation coatings on AM50 magnesium alloy, Surface Engineering 26 (2010) 367–370.

[19] H.M. Wang, Z.H. Chen, Y.L. Cheng, Optimisation of anodising electrolyte for magnesium alloy AZ31 and characteristics of anodic film, Surface Engineering 26 (2010) 334–339.

[20] J.A. Curran, T.W. Clyne, Porosity in plasma electrolytic oxide coatings, Acta Materialia 54 (2006) 1985–1993.

[21] J.A. Curran, T.W. Clyne, Thermo-physical properties of plasma electrolytic oxide coatings on aluminium, Surface and Coatings Technology 199 (2005) 168–176.

[22] J.M. Wheeler, C.A. Collier, J.M. Paillard, J.A. Curran, Evaluation of micromechanical behaviour of plasma electrolytic oxidation (PEO) coatings on Ti–6Al–4 V, Surface and Coatings Technology 204 (2010) 3399–3409.

[23] M. Datcheva, S. Cherneva, M. Stoycheva, R. Iankov, D. Stoychev, Determination of anodized aluminum material characteristics by means of nanoindentation measurements, Materials Sciences and Applications 2 (2011) 1452–1464.

[24] A. Ghasemi, V.S. Raja, C. Blawert, W. Dietzel, K.U. Kainer, Study of the structure and corrosion behavior of PEO coatings on AM50 magnesium alloy by electrochemical impedance spectroscopy, Surface and Coatings Technology 202 (2008) 3513–3518.

[25] M. Stern, A.L. Geary, Electrochemical polarization: I. A theoretical analysis of the shape of polarization curves, Journal of the Electrochemical Society 104 (1957) 56–63.

[26] W.C. Oliver, G.M. Pharr, An improved technique for determining hardness and elastic modulus using load and displacement sensing indentation experiments, Journal of Materials Research 7 (1992) 1564–1583.

[27] H. Zhou, F. Li, B. He, J. Wang, B. Sun, Air plasma sprayed thermal barrier coatings on titanium alloy substrates, Surface and Coatings Technology 201 (2007) 7360–7367.
[28] D. Basu, C. Funke, R.W. Steinbrech, Effect of heat treatment on elastic properties of separated thermal barrier coatings, Journal of Materials Research 14 (1999) 4643–4650.
[29] S. Guo, Y. Kagawa, Effect of thermal exposure on hardness and Young's modulus of EB-PVD yttria-partially-stabilized zirconia thermal barrier coatings, Ceramics International 32 (2006) 263–270.
[30] A. Dey, A.K. Mukhopadhyay, S. Gangadharan, M.K. Sinha, D. Basu, N.R. Bandyopadhyay, Nanoindentation study of micro-plasma sprayed hydroxyapatite coating, Ceramics International 35 (2009) 2295–2304.
[31] A. Dey, A.K. Mukhopadhyay, S. Gangadharan, M.K. Sinha, D. Basu, Weibull modulus of nano-hardness and elastic modulus of hydroxyapatite coating, Journal of Materials Science 44 (2009) 4911–4918.
[32] X. Nie, E.I. Meletis, J.C. Jiang, A. Leyland, A.L. Yerokhin, A. Matthews, Abrasive wear/corrosion properties and TEM analysis of Al_2O_3 coatings fabricated using plasma electrolysis, Surface and Coatings Technology 149 (2002) 245–251.
[33] Q. Dong, C.Z. Chen, D.G. Wang, Q.M. Ji, Microstructure and element distribution in thin MgO coatings on pure magnesium by microarc oxidation, Surface Engineering 22 (2006) 177–180.
[34] A.H. Ucisik, S. Durdu, Investigation of mechanical properties of AZ31 Mg alloys coated by plasma electrolytic oxidation, International Symposium on 'Magnesium Technology 2012', TMS Annual Meeting and Exhibition, March 11–15 (2012) Orlando, FL.
[35] V.V. Narulkar, S. Prakash, K. Chandra, Ceramic coated Y1 magnesium alloy surfaces by microarc oxidation process for marine applications, Bulletin of Materials Science 30 (2007) 399–402.
[36] D.Y. Hwang, K.R. Shin, B. Yoo, D.H. Lee, D.Y. Park, D.H. Shin, Characterization of plasma electrolytic oxide formed on AZ91 Mg alloy in $KMnO_4$ electrolyte, Transactions of the Nonferrous Metals Society of China 19 (2009) 829–834.